AIAA JOURNAL
Vol. 44, No. 5, May 2006

Unsteady Periodic Behavior of a Disturbed Tip-Leakage Flow

Ruolong Ma* and William J. Devenport†
Virginia Polytechnic Institute and State University, Blacksburg, Virginia 24061-0203

The unsteady periodic behavior of a tip-leakage flow downstream of a simulated axial compressor rotor has been studied. A linear cascade wind tunnel has been adapted to model this situation. The wind tunnel features a moving endwall to simulate the relative motion between the rotor and casing and vortex generators attached to the moving end wall that produce an idealized periodic unsteady vortical inflow simulating the flow shed by the casing junctions of a row of inlet guide vanes. Detailed three-component mean-velocity and turbulence measurements have been made just downstream of the blade trailing edges and phase averaged with respect to the relative position of the blades and vortex generator wakes. The comparison between the disturbed and undisturbed tip-leakage flows shows that on time average the vortical inflow does not change the flowfield much, except for a slight decrease in streamwise velocity deficit and a small increase in turbulence kinetic energy in the tip-leakage vortex region. However, phase-averaged measurements reveal that the inflow vortices produce significant fluctuations in the size, strength, structure, and position of the tip-leakage vortex, despite the fact that they are about two orders weaker than the tip-leakage vortex. It is hypothesized that the unsteady vortical inflow influences the tip-leakage vortex at its formation, by periodically disturbing the shedding of vorticity from the blade tip.

Introduction

THIS study mainly concerns unsteady tip-leakage flow produced in a ducted propulsion pump or axial compressor. As shown in Fig. 1, the rotor of an axial propulsion pump often operates downstream of a set of fixed stators or inlet guide vanes. The inlet guide vanes produce wakes that near the casing can be dominated by necklace and/or casing-separation vortices. These wakes create an unsteady inflow to the rotor, which can have a large influence on the downstream rotor and downstream flow. For example, the inflow will create unsteady lift and thus vibration of the rotor blades; it can stimulate time-dependent transition in the rotor-blade boundary layers; it can also influence other viscous structures such as the tip-leakage vortices shed from the rotor-blade tips. What happens to the rotor tip-leakage vortices in this situation is of some importance. If the inlet guide vane wakes stimulate fluctuations in the size, strength, form, or position of the tip-leakage vortices, then these can substantially alter the rate of heat transfer to the casing wall, the noise and vibration produced when the vortices impinge on downstream elements, etc. In propulsion pumps such motion of the tip-leakage vortex is thought to be associated with intermittent microscopic cavitation.

There are several reasons to believe that the tip-leakage vortices will be susceptible to inflow disturbances. First, they are formed by the rolling up of fluid separating from the salient edge of the blade tip. Such separations are notoriously sensitive. Second, the stator wake vortices must periodically pass through the rotor-blade tip gap. The rapid acceleration of the flow here is likely to greatly intensify these vortices. Third, in most configurations the time taken for a given rotor blade to traverse the distance between two successive stator wakes is comparable to the time taken for fluid in the tip-leakage vortex to convect the length of the blade passage. One would expect tip-leakage vortices to be particularly sensitive to disturbances on this timescale.

Received 8 July 2004; revision received 2 September 2005; accepted for publication 6 September 2005.

*Graduate Assistant, Department of Aerospace and Ocean Engineering; currently Research Associate, Hessert Laboratory, Aerospace and Mechanical Engineering Department, University of Notre Dame, Notre Dame, IN 46556. Senior Member AIAA.

†Professor, Department of Aerospace and Ocean Engineering, 215 Randolph Hall. Senior Member AIAA.

Despite its importance, the literature contains few references to studies of this aspect of stator-rotor interaction. Many studies[1–5] of stator rotor interaction concentrate only on the unsteady transition of the rotor-blade surface boundary layer and unsteady passage flow. A few studies have been concerned with the unsteady tip-leakage vortex. These include Poensgen and Gallus,[6] who made measurements, using five-hole and triple-hot-wire probes, downstream of an annular stator with tip gap operating in the wake of a rotor with rotating cylinders located about 50% of blade chord upstream. They found there were periodic changes in the intensity of the tip-leakage vortex, which they attributed to a periodic change in stator blockage associated with a pulsating corner stall at the hub.

Yamamoto et al.[7] made single hot-wire measurements at 11 planes before, within, and after the second-stage stator passage of a 1.5-stage axial-flow turbine. The authors found that the stator tip-leakage vortex is influenced by the rotor-stator interaction, and its size and strength change with time. They also found a secondary vortex rotating counter-clockwise near the hub endwall was also unsteady, and the center of the vortex approaches and departs from the hub endwall.

Zeschky and Gallus[8] performed measurements to study the effects of stator wakes and spanwise nonuniform inlet conditions on the rotor flow of an axial turbine stage by using pneumatic five-hole probes and triple/X-hot-wire probes. The authors hypothesized that the formation of the tip-leakage and passage vortices is strongly influenced by the spanwise nonuniform stator outlet flow. They measured the highest fluctuations of velocity, flow angle, and turbulence intensity in the hub and tip regions. However, no correlation for a quantitative assessment of the unsteady effects was derived from the data.

Gallus et al.[9] investigated the endwall and unsteady flow in an axial turbine stage by using three-dimensional hot-wire and pneumatic probes. They also performed three-dimensional Navier–Stokes steady and unsteady numerical analysis. The comparison showed that the unsteady flow calculation gives much better results for the time-averaged secondary flowfield at the exit of the rotor. The study indicated that the passage vortex near the hub of the rotor is transported toward the midspan because of the blade interaction effects, and the structure of the secondary flowfield at the exit of the rotor is significantly modified by the unsteady effects.

Wernet et al.[10,11] studied the rotor tip clearance flow downstream of an inlet guide vane in an axial compressor using three-component digital particle image velocimetry (DPIV). Three-component steady flow measurements were made in the blade tip region in the top 10% of the span at 2% span increments at two conditions: design mass flow and a mass flow coefficient just above compressor stall.

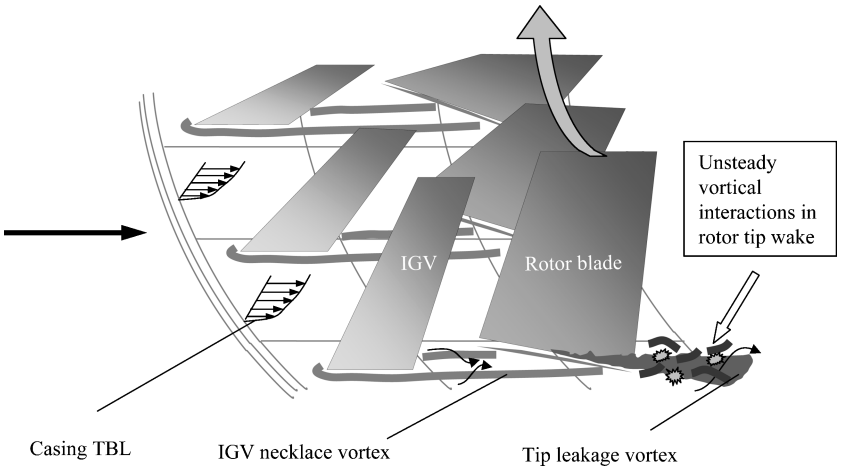

Fig. 1 Schematic of a stator-rotor-casing interaction.

The three-component measurements showed reasonable agreement with the computational fluid dynamics (CFD) prediction of the tip clearance flow at the design operating point except that the DPIV data showed the tip clearance vortex extends radially farther down into the blade passage than the CFD prediction at the design mass flow. At a mass flow just above stall, the DPIV data showed the tip clearance leakage flow develops a large blockage region extends throughout the top 10% of the blade passage.

In brief, the preceding studies clearly indicate that stator-rotor interaction is likely to produce unsteady motions in the tip-leakage vortices; however, most results just provide time-averaged formation and development of the vortex structures. Some studies provide limited unsteady motion information, but none of them provides much detail of the causes or characteristics of the unsteady changes or of the turbulent flow structure with which they are associated. This comes in part from the fact that all of this work has been done on rotary turbomachines where the scale of the tip-leakage flows tends to be small and measurements usually cannot be made in a rotating frame. In addition, the complicated geometrical configuration makes the flow in rotary turbomachines be subject to so many factors that the involved mechanisms of the unsteady motion become hard to separate.

Prior work involving unsteady tip-leakage vortices in water flows has centered on the high-Reynolds-number pump facility at the Pennsylvania State University. Experiments and computations have been performed,[12–17] but again the most part of these results reveals only the time-average formation and development of the vortex structures and does not reveal the mechanism or consequences of their unsteady interaction. One exception is the flow visualizations of Zierke et al.,[12,13] which show dramatic wandering and kinking of the cavitating tip-leakage vortex as it passes downstream of the rotor-blade trailing edge, perhaps as a consequence of the vortical interaction just hypothesized.

The objectives of the current study are 1) to simulate the unsteady tip-leakage vortex motion associated with stator-rotor interaction in an idealized environment free of confounding influences and where measurements are easily made; 2) to reveal and quantify the unsteady behavior of the tip-leakage vortices through phase-averaged measurements; and 3) to improve the understanding of the mechanisms involved.

To achieve these objectives, we are using a low-speed linear cascade wind tunnel at Virginia Polytechnic Institute and State University. This facility has a unique high-speed moving endwall that reproduces the relative velocity between the casing and blade tips found in a rotor flow. The cascade produces a large-scale tip-leakage flow, and measurements can easily be made in the physically important rotor frame. However, simulating the effects of a set of inlet guide vane wakes on the cascade in this facility poses an obvious difficulty. Fortunately, we found that the vortex generators attached to the moving endwall can be used to produce an unsteady vortical inflow to the cascade that simulates, in an idealized way, the wakes shed at the junctions of the inlet guide vanes and the casing.

In analyzing the effects of stator-rotor interaction on the rotor tip flow, it is important to realize that the stator wakes will almost always be skewed relative to the rotor-blade leading edges and thus will trace along them as the blades rotate. The most important part of the interaction, from the point of view of the tip-leakage vortices, will therefore occur when the blade tips pass through those sections of stator wake formed closest to the casing. Necklace, corner separation, and other secondary flow vortices generated at the junction of the stators and casing will dominate these parts of the stator wakes. Those parts of this flow lying closest to the casing will likely have the greatest effect on the tip-leakage vortex because it is these that directly interact with the blade tip from which the leakage vortex is shed. So in this sense, using the vortex generators to model the inlet guide vane wakes is reasonable.

The moving wall cascade with vortex generator model is undoubtedly different from real turbomachines in many other respects, such as lack of axisymmetric effects, curvature of the casing, secondary flow inside the boundary layer on the rotor blades generated by rotation-induced centrifugal and Coriolis forces, etc. However, it is our hypothesis that the influences on the unsteady tip-leakage vortex caused by these differences will not affect the basic mechanism of the unsteady motion of the tip-leakage vortex. The mechanism of this flow phenomenon can easily be studied in this idealized situation.

More details of this study are described by Ma.[18] There are a number of studies related with the present work. Kuhl,[19] Tian,[20] and Tang[21] studied the same tip-leakage flow produced by the same facility using laser Doppler anemometry and focusing on the near-wall flow. Mish[22] investigated the unsteady loading caused by the inflow disturbance near the blade tip of same facility by embedding a microphone array into the blade surface.

Apparatus and Techniques

Cascade Wind Tunnel with Moving Wall

The low-speed linear cascade wind tunnel was built by Muthanna and Devenport[23] to study tip-leakage vortices. A moving-wall system to simulate the relative motion between rotor blades and casing was added by Wang and Devenport.[24] It was further modified in current study to adapt it for the attachment of vortex generators to the moving wall.

Figure 2 is a schematic of the test section after modification. The blade inlet angle is 65.1 deg. The stagger angle of the cascade is 56.9 deg. The cascade consists of eight cantilevered GE rotor B section blades mounted on a structure that allows individual adjustments for each tip gap. The blades have a chord length of 254 mm and effective span of nearly the same depending on the size of the tip gap. The blade spacing s is 236 mm, and tip gap used in this

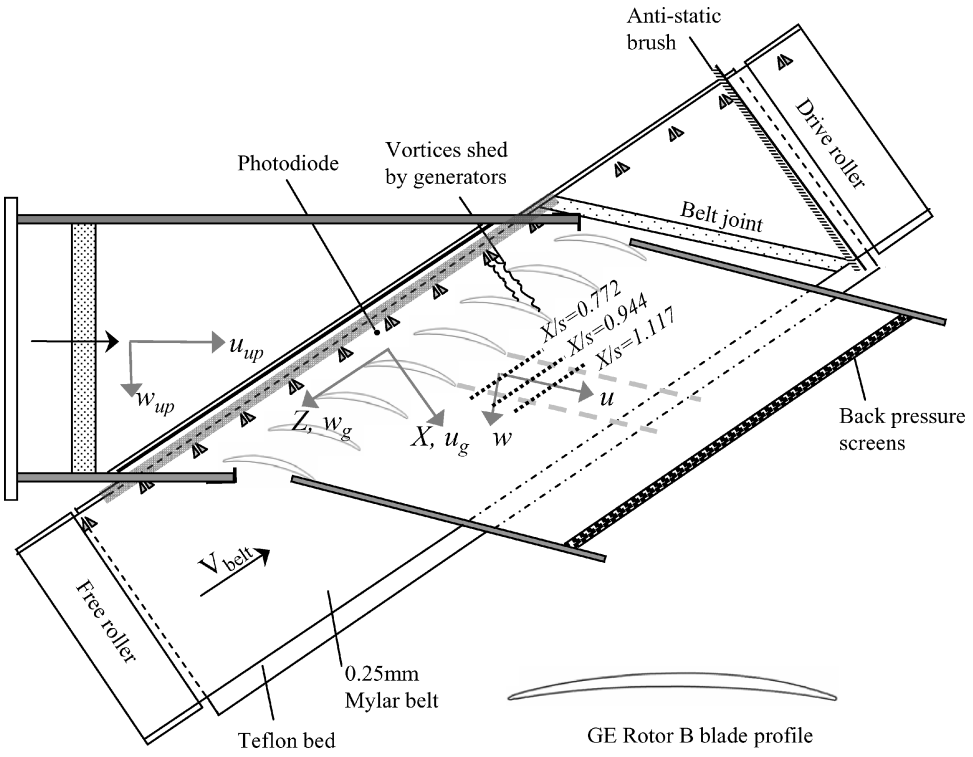

Fig. 2 Plan view of the Virginia Tech cascade wind-tunnel test section: dimensions in millimeters and not to scale.

experiment was 8.38 mm (3.3% of the chord). Boundary-layer trips, 6.4 mm wide (0.51-mm-diam glass sanding beads spread in a single layer), were attached on both sides of each blade at 25.4 mm downstream of the blade leading edge to eliminate any undesirable effects caused by natural boundary-layer transition.

Flow enters the cascade row with the boundary layer being removed by two suction slots on the upper and lower end walls. Underneath the blade row, there is a moving endwall, a 0.254-mm-thick Mylar belt driven using a 15-hp ac synchronous motor over the lower end wall. The belt is 686 mm wide, with windward edge covered to prevent it from lifting inside of the tunnel. On the upper endwall of the downstream section, seven 8-mm-wide pitchwise traverse slots were cut with a spacing of 46 mm in the axial direction. A 0.1-mm-thick tape was affixed over the slots to minimize flow leakage. Hot-wire or microphone probe holders can be inserted through these traverse slots to make measurements. Three screens fitted at the section exit raise the pressure at the cascade inlet to about 9 mm of water above atmospheric so that the suction slots operate as designed. Adjustable angle tailboards were used to guide the flow downstream of the cascade. The blade shape and cascade configuration of this wind tunnel were found to be able to represent the flow in propulsion pump rotors or compressor rotors.

The facility was modified for the present study by moving the blade row to a position 189 mm axially downstream of the suction slot leading edge to allow room for the vortex generators. The belt extends about 125 mm axially upstream and 422 mm axially downstream of the blade row after modification. The tunnel inlet section floor was further modified to introduce a porous strip (63.5 mm wide, spanning the section) to ensure the boundary layer on the floor could be completely removed at the tangential suction slot without imposing any pressure gradient on the flow here. As shown in Fig. 3, a new, more severe, boundary-layer trip wire of rectangular cross section (2.4×2.4 mm) was introduced 7 mm downstream of the bottom suction slot leading edge to increase the thickness of the lower endwall boundary layer entering the cascade. A Teflon® sheet flushed into the lower endwall was introduced to reduce the friction and active suction was used to hold the belt on the Teflon bed. Antistatic brushes, mounted on top and underneath the belt just outside the wind tunnel, were used to prevent a buildup of static electricity.

In the present cascade configuration the nominal inlet freestream velocity was 24.5 ± 0.5 m/s. The tailboards were adjusted to a turning angle of 11.8 deg at which the flow was free from any net pitchwise pressure gradient. The chord Reynolds number at 27°C was about $3.98 \times 10^5 \pm 8.1 \times 10^3$. The design belt speed equals the pitchwise component of the freestream of the inflow. With normal freestream velocity of 24.5 m/s, the belt speed was held constant at 22.2 m/s with an uncertainty of $\pm 1\%$. The measured rms axial drift of the belt was less than ± 4.5 mm and at most times much less. According to Kuhl,[19] the rms vibration of belt (not including the belt joint jump) is 6.58 μm, and the belt joint jump displacement is larger than 100 μm. The belt joint, a 70-mm-wide strip skewed at an angle between 40 to 45 deg with doubled thickness, produced the greatest fluctuations in instantaneous tip gap. However, measurements made in vicinity of the belt joint were eliminated in postprocessing.

Vortex Generators

Half-delta-wing vortex generators pairs, shown in Fig. 4, were used to model the inlet guide vane wakes in an idealized way. The vortex generators, based on the design of Pauley and Eaton,[25] were made of 0.5-mm-thick sheet metal, have an axial chord length of 24 mm, height of 10 mm, and angle of attack of ± 18 deg. They were placed 20 mm apart at midchord in pairs so as to produce a "common-flow down" counter-rotating vortex pair: an idealization of a necklace vortex wake. The axes of the generator pairs were aligned perpendicular to the blade row because, in the frame of reference moving with the belt, this is the direction of the freestream. The counter-rotating vortices shed by the generators then grow in the axial direction as they are translated tangentially with the belt.

The vortex generators were glued to the belt with their trailing edges 68.6 ± 4.5 mm upstream of the blade row to generate an unsteady periodic vortical inflow representative of an array of stator necklace vortices. The uncertainty in location reflects the limits of the axial drift of the belt. Except at the belt joint, the spacing between successive pairs of generators was set equal to the blade spacing so that the unsteady boundary conditions of the flow would be periodic (an important consideration for computors). The inevitable uneven spacing interval was arranged to coincide with the belt joint that

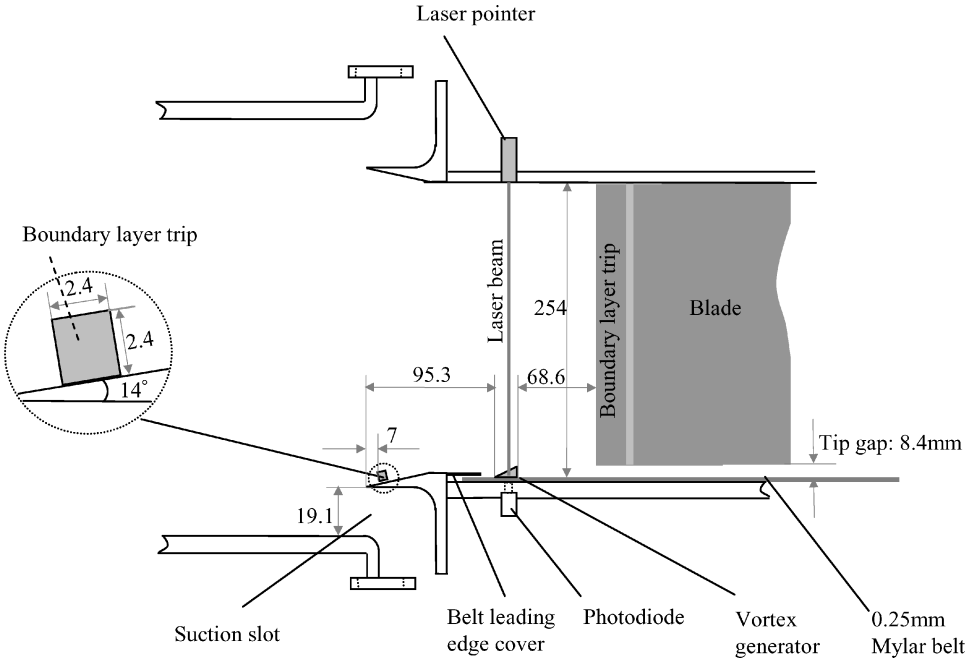

Fig. 3 Cross section through the cascade taken along the cascade axial direction: dimensions in millimeters and not to scale.

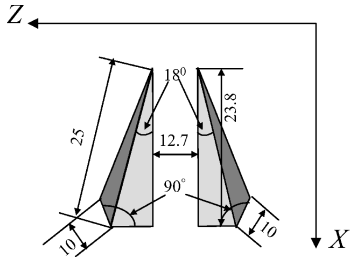

Fig. 4 Delta-wing vortex generator pair.

provided a means for detecting the passage of the joint (see the following).

A photodetector, shown in Fig. 3, was embedded in the Teflon bed underneath the belt at a location 81 mm axially upstream of the center of the cascade leading-edge line (i.e., directly in the path of the vortex generators). The detector was illuminated with a laser beam shone vertically downward from outside the tunnel through the clear Mylar belt, the beam being interrupted by the passage of the vortex generators. The detector signal was amplified and sampled simultaneously with hot-wire measurements. It was then postprocessed 1) to identify and eliminate any measurements made during the passage of the belt joint; 2) to determine the time intervals between the passage of generator pairs, and thus the near-instantaneous belt speed; and 3) to construct a phasing signal by subdividing each time interval into 256 equal periods representing the instantaneous position of the vortex generator pairs relative to the blades. The resolution in the phasing signal corresponds to $236/256 = 0.92$ mm of vortex generator movement. The rms variation in belt speed inferred using this method was 0.24%. This figure is low enough that we suspect it contains a significant contribution from the uncertainty in the placement of the generator pairs on the belt. (Then 0.24% in this case would correspond to a position uncertainty of 0.6 mm.)

Hot-Wire Anemometry

Velocity measurements were made using a computerized hot-wire system described in detail by Wittmer et al.[26] and Devenport et al.[27] Miniature four-sensor hot-wire probes manufactured by Auspex Corporation (type AVOP-4-100) were used. These probes consist of two orthogonal X-wire arrays with each sensor inclined at a nominal 45-deg angle to the probe axis. The total measurement volume is approximately 0.5 mm^3. All sensors were operated separately using a Dantec 56C17/56C01 constant-temperature anemometer unit. Anemometer bridges were optimized to give a matched frequency response greater than 25 kHz. The probe was calibrated for velocity before and after the measurements by placing it in the uniform jet of a TSI calibrator and a direct angle calibration (lookup table) method, described in detail by Wittmer et al.,[26] was used to obtain the three velocity components. For inflow boundary-layer measurements, a Model 1218 standard boundary-layer probe from TSI was used. The probe was mounted with the sensor parallel to the endwall and using a holder that permitted the probe to be yawed to different angles about the center point of the sensor.

A Hewlett Packard E1432A 16-channel digitizer, with a maximum sampling frequency of 51,200 Hz per channel at 16-bit resolution, was used for data acquisition. A computer-controlled two-axis traverse system with a resolution of 0.025 mm was used position probes. All data acquisition and traversing were controlled from a single Pentium computer using programs written in Agilent VEE.

At measurement locations where only time-average results were required, the hot-wire signals were sampled in a single record of 10,240 samples at a rate of 1600 Hz. For phase-average measurements, however, 100 records of 16,384 samples of the hot-wire signals and generator phasing signal were recorded at a rate of 25.6 kHz. This sampling rate was chosen to ensure that at least 256 samples would be recorded during each generator pair passage, and thus each such passage could be subdivided into 256 phases. The record length 16,384 was chosen so that each record would contain a continuous set of data from more than one complete revolution of the belt. The total number of samples was chosen so that the phase averages would be based on about 4600–4800 vortex generator pair passes after unusable parts of the signals, that is, the uneven vortex generator pair interval or passages for which the generator signal had irremovable noise, were ignored. Phases were numbered starting with zero for the time instant when each generator pair was centered axially upstream of the center point of each blade passage entrance. Thus, at phase 128, generator pairs are located axially upstream of the blade leading edges. Time-series measurement data were ensemble averaged based on each phase time to obtain the phase-averaged statistics.

The uncertainties were calculated for 20:1 odds using the method of Kline and McClintock.[28] Table 1 gives the uncertainty estimates for mean velocity, turbulence kinetic energy, and streamwise vorticity. These estimates apply both to the time- and phase-average results.

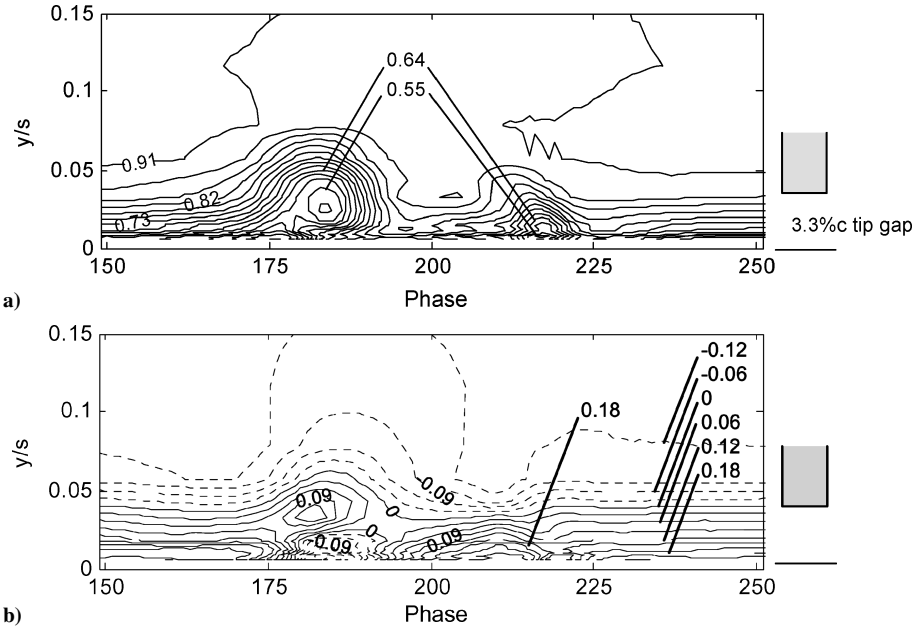

Fig. 5 Measured inflow mean velocity at $X/s = -0.135$: a) contours of phase-averaged $\langle u_g \rangle / U_{eX}$ in steps of 0.03 from 0.4 to 1 and b) contours of phase-averaged $\langle w_g \rangle / U_{eX}$ in steps of 0.03 from −0.3 to 0.3. Negative levels are shown dashed. Tip gap of 3.3% chord is plotted to scale.

Table 1 Measurements uncertainties

Quantity	Uncertainties (20:1 odds), %
Single-wire phase-averaged measurements	
$\delta(\langle u \rangle, \langle w \rangle)/U_e$	4
Quad-wire time- and phase-averaged measurements	
$\delta U/U_\infty$	1
$\delta(V, W)/U_\infty$	0.7
$\delta(\overline{u'^2}, \overline{v'^2}, \overline{w'^2})/U_\infty^2$	0.01, 0.08, 0.1
$\delta(\overline{u'v'}, \overline{v'w'}, \overline{u'w'})/U_\infty^2$	0.005, 0.03, 0.02
$\delta k/k$	6
$\delta(\Omega_x)/\Omega_x$	18

Results and Discussion

In presenting measurements we will use cascade aligned coordinates (X, y, Z) of Fig. 2 and of Muthanna and Devenport[23] to define axial, spanwise, and pitchwise positions from an origin located on the lower end wall midway between the leading edges of the two center blades of the cascade (blades 4 and 5). The cascade inflow and outflow make angles of 65.1 and 53.3 deg, respectively, with the X direction. Coordinates are normalized on the blade spacing s of 236 mm. Velocities are normalized on the inlet freestream velocity U_∞ except being indicated otherwise.

Vortical Inflow

The inflow generated by the vortex generators in the cascade tunnel was first investigated to obtain the flow conditions experienced by the tip-leakage vortex.

Phase-average measurements were made by using a single-wire boundary-layer probe because it can approach the wall more closely than the four-sensor probe. A rotation technique was used to measure the two velocity components parallel to the endwall and the corresponding Reynolds stresses.[18] The measurement location ($X/s = -0.135$, $Z/s = 0.263$) was on the central streamline of the central passage (between blades 4 and 5) and 31.8 mm (0.135 s) upstream of the blade-row leading edge. It was also 36.9 mm (0.16 s) downstream of the trailing edge of the vortex generators. The single hot-wire probe was yawed at three different angles 0, −32.55, and −65.1 deg relative to the inlet flow direction, and the measurements made were reduced to obtain the desired quantities using the measured yaw calibration of the probe.

The inflow measurement result is presented in Fig. 5 in terms of the phase-averaged axial and pitchwise velocity components $\langle u_g \rangle$ and $\langle w_g \rangle$ normalized by the axial component of the local edge velocity U_{eX}. Note that the speed of the moving endwall has been subtracted from the pitchwise velocity component, and thus these pictures show the flow as seen from a frame of reference moving with the vortex generators. Based on the endwall speed, the time interval between phases 149 to 251 represented here corresponds to a belt movement of pitchwise distance of $0.4s$, thus, this y vs phase plot can be interpreted as a y vs Z_b plot, where Z_b is the pitchwise position of the belt. The plot aspect ratio has been set so that equal distances along the horizontal and vertical axes represent equal distances in y and Z_b so that the physical shape of the flow is revealed. In Fig. 5 two counter-rotating vortices are clearly visible through the axial-velocity defect and crossflow velocity variations they produce. In the $\langle u_g \rangle$ contours, two deficit regions are seen centered at phase numbers 184 and 218, respectively. The leading one (at phase number 184) is larger, and also has larger velocity deficit of $0.48U_{eX}$ than that of the trailing one. In the $\langle w_g \rangle$ contours, there is a visible pattern consistent with counter-rotating vortices, the leading vortex being clockwise and the trailing one being anticlockwise. However, the plot also shows significant skewness within the boundary layer to either side of the vortices. There is a positive peak in $\langle w_g \rangle$ of $0.24U_{eX}$ near the wall and a negative one of $-0.12U_{eX}$ outside the boundary layer. It is this skewness in combination with the vortex generators that makes the two counter-rotating vortices asymmetric. As explained in detail by Ma,[18] the skewness of the boundary layer is caused by relative motion between the moving belt and the stationary leading-edge part of the lower endwall. The negative $\langle w_g \rangle$ outside the boundary layer is seen because the measurement location is fairly close to the leading edge of the blades and the flow is already showing some turning by the blades.

The circulation of the vortices was estimated based on the three-component hot-wire measurements made by Ma[18] and LDV measurements made by Kuhl and Simpson[29] in a small boundary-layer tunnel that was designed to reproduce the axial flowfield in the cascade tunnel. The measurements show the total circulation in each of the vortices to be about $0.003U_\infty s$, where U_∞ is the freestream velocity in the cascade tunnel and s is the blade spacing. As shown later, the circulation is about two orders of magnitude smaller than the typical circulation in the tip-leakage vortices in the cascade tunnel.

The inflow boundary-layer profiles were determined by taking average of the boundary-layer data from phase 1 to 128, which are undisturbed by the vortex generators. The results show that in the frame of reference moving with the endwall the boundary layer has a thickness of $0.06s$. Again, the boundary layer is skewed, and the flow there is already turned by the blades as it approaches the blades.

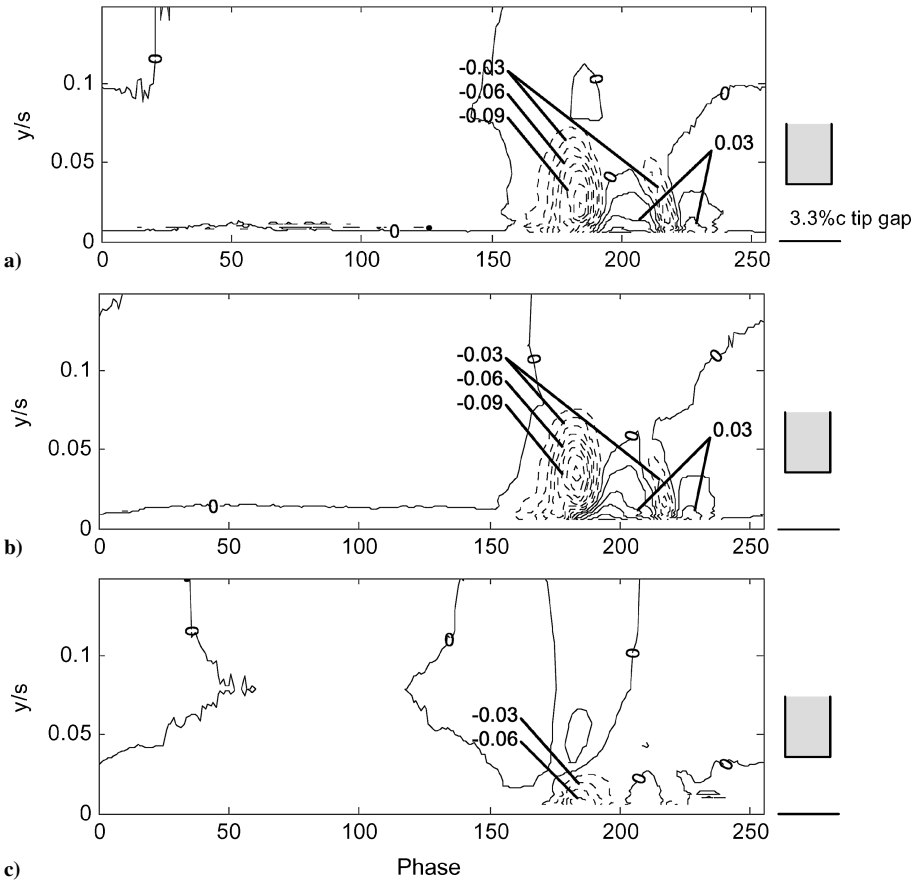

Fig. 6 Inflow upwash ($\langle w_{up} \rangle - W_{up})/U_e$ at $X/s = -0.135$: a) contours of total upwash, b) contours of upwash caused by axial component velocity deficit, and c) contours of upwash caused by pitchwise vortical component. Contours are in steps of 0.015 from −0.15 to 0.15. Negative levels are shown dashed. Tip gap of 3.3% chord is plotted to scale.

These data are presented again in terms of blade relative upwash velocity in Fig. 6. Specifically this plot shows the phase-averaged velocity perpendicular to the freestream direction $\langle w_{up} \rangle$ in the frame of reference of the blades (see Fig. 2). The time-average velocity in this direction W_{up} has been subtracted so that only the unsteady periodic upwash is seen. The upwash is expected to cause the unsteady loading on the blades and is required for an inviscid calculation (e.g., Glegg[30]) of the inviscid blade response.[22] Figure 6a shows the total phase locked upwash fluctuation. Strong negative upwash followed by smaller positive upwash can be seen to be generated by each of the inflow vortices region. Figures 6b and 6c show the contributions to this upwash from the axial $\langle u_g \rangle$ and pitchwise $\langle w_g \rangle$ velocity fluctuations shown in Fig. 5. The contribution from the axial component velocity deficit is clearly dominant. This suggests that in the turbomachinery situation, instead of the pitchwise and spanwise fluctuations, the axial-velocity deficit might be the major source of unsteady loading on the downstream blade tips.

Cascade Outflow: Time-Averaged Results

Before presenting the results of tip-leakage vortex disturbed by the vortical inflow, it is necessary to summarize the previous studies of the undisturbed tip-leakage vortex conducted in this facility.

Muthanna and Devenport[23] studied the structure of a tip-leakage vortex and its trajectory downstream of the cascade at different tip gaps. The measurements reveal that the vortex is a region of strong streamwise velocity deficit, but weaker rotating motion. Turbulence kinetic energy in the vortex appears to be produced almost entirely by the velocity gradients associated with the deficit. Further insight into this vortex structure was provided by the analysis of Wenger et al.,[31] who considered the two-point turbulence measurements made in Muthanna and Devenport's tip-leakage vortex downstream of the cascade. Wenger et al. found that the leakage vortex is not subject to low-frequency wandering motions. The turbulence in the tip-leakage vortex is highly anisotropic and characterized by elongated eddies inclined at about 30 deg to the vortex axis. Wang and Devenport[24] enhanced the facility by adding a moving wall to correctly simulate the relative motion between the blade tips and endwall. Wang and Devenport found that wall motion influences the leakage vortex by flattening and shearing the turbulence and mean velocity distributions of the vortex but does not alter the basic mechanisms that govern the development of its mean flow and turbulence structure. Muthanna[32] made further studies to examine the flow's behavior both in the presence and absence of grid-generated freestream turbulence. Significant effects on the flowfield as a result of the grid-generated turbulence were revealed, which include a 4% decrease in blade loading, a 20% reduction in the vorticity levels within tip-leakage vortex, a 30% increase in size of tip-leakage vortex, and a shift to the suction side in the vortex path.

In the current study, tip-leakage flow measurements were made at $X/s = 0.944$, 84 mm axially downstream of center passage of the cascade. Phase-averaged measurements were obtained over a smaller, more detailed grid, covering the tip-leakage flow region and its unsteady motion. The grid has a minimum size of ($\Delta y = 0.022s$, $\Delta Z = 0.054s$) starting from $0.011s$ to $0.1s$ above the wall and then gradually becomes less dense from $0.1s$ to $0.3s$. This resolution is adequate for most of the important flow features. Near-wall features ($y < 0.011s$) could not be resolved, however, because of the difficulty of probing close to the moving belt. The objective here was to obtain phase-averaged statistics, and more time-averaged data of unsteady flow. Time-averaged measurements were made outside the tip-leakage vortex region, where there are no obvious unsteady phenomena.

These data are presented in terms of streamwise, spanwise, and lateral velocity components (u, v, w) aligned with the potential core flow downstream of the cascade (see Fig. 2). Time-averaged measurements, with and without vortex generators, are presented in Figs. 7–10 in terms of contours of mean streamwise velocity, mean crossflow velocity vectors, turbulence kinetic energy, and mean

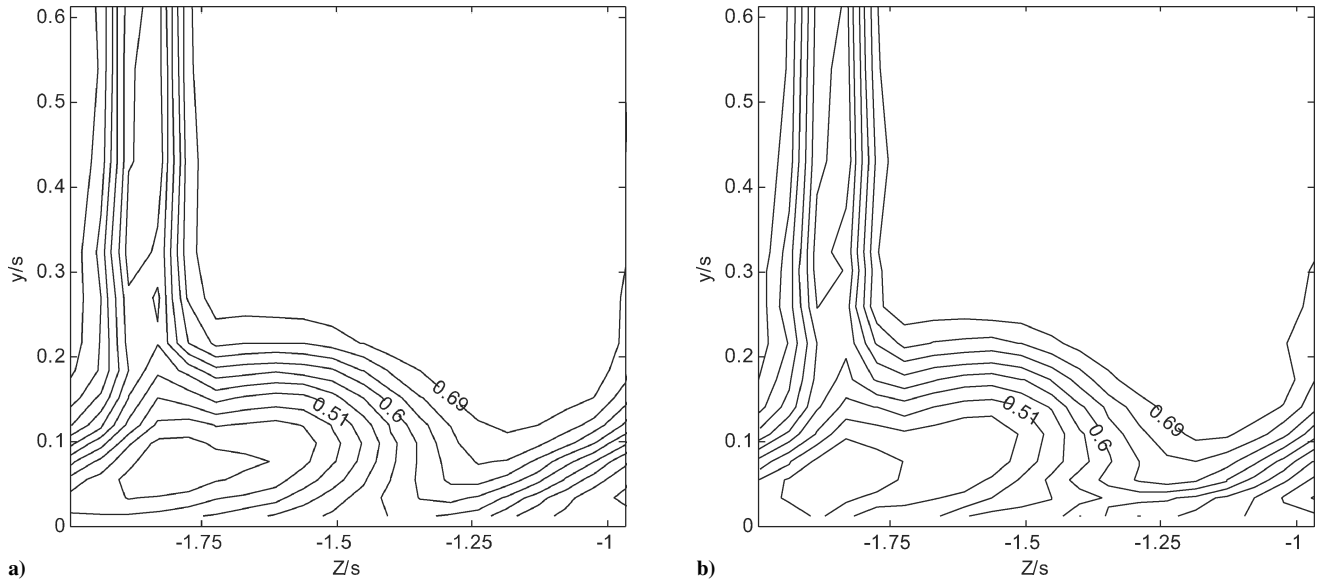

Fig. 7 Contours of time-averaged U/U_∞ at $X/s = 0.944$: a) without vortex generators and b) with vortex generators. Contours in steps of 0.03 from 0.3 to 0.7.

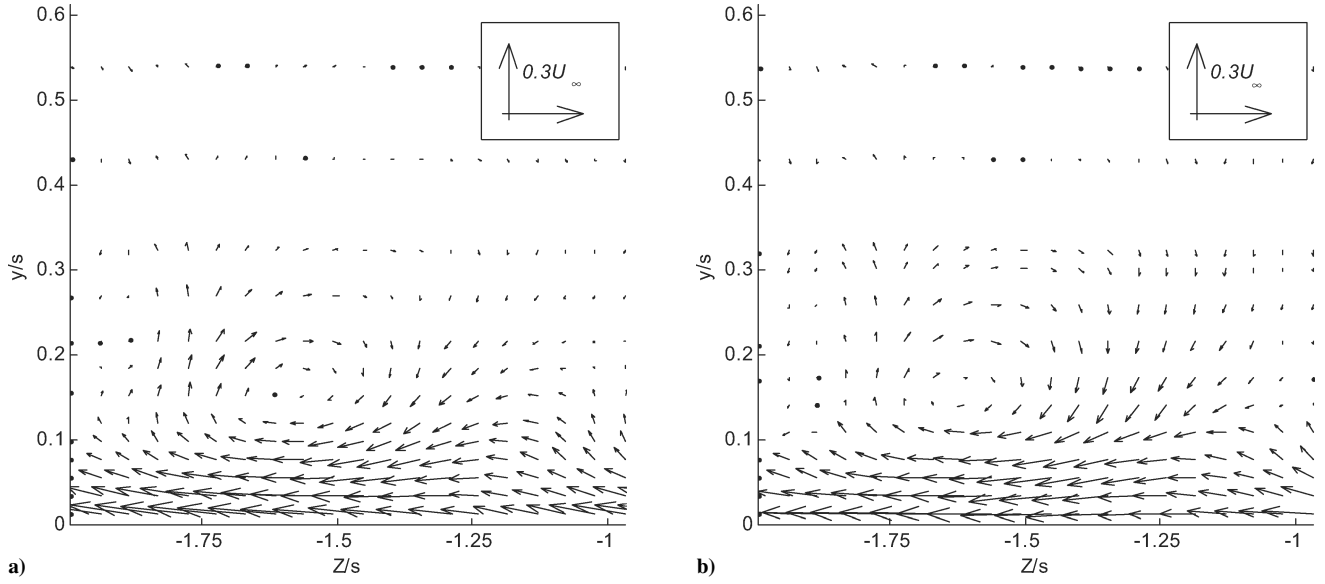

Fig. 8 Vectors of mean crossflow velocity (V, W) at $X/s = 0.944$: a) without vortex generators and b) with vortex generators.

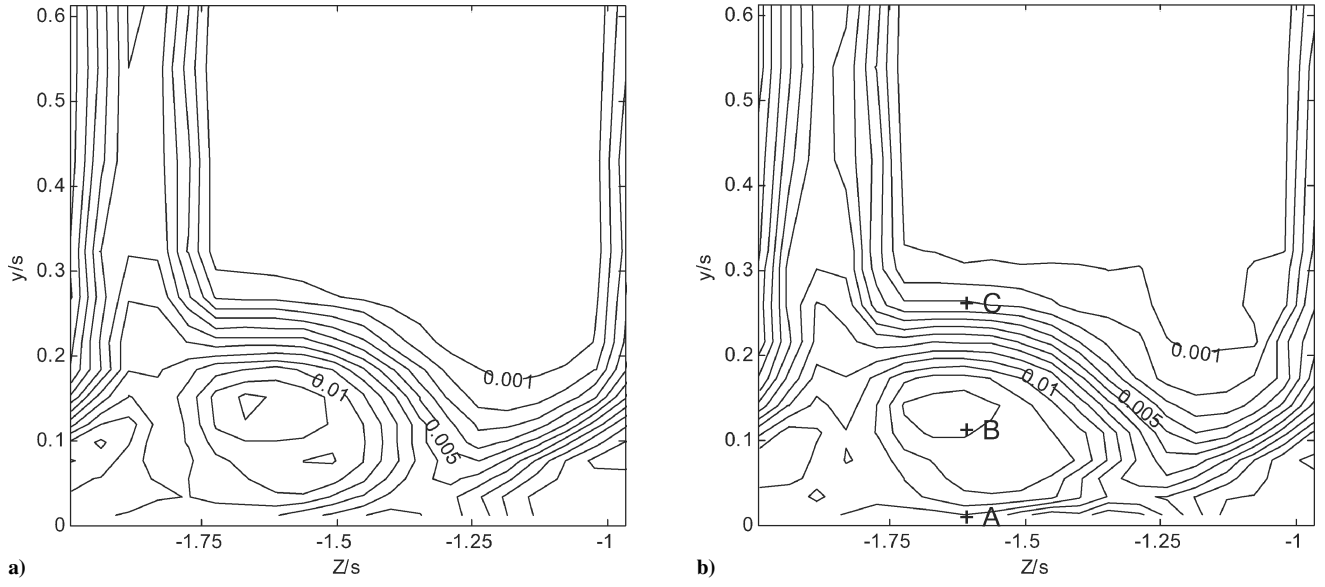

Fig. 9 Contours of turbulence kinetic energy k/U_∞^2 at $X/s = 0.944$: a) without vortex generators and b) with vortex generators. Contours are in steps of 0.001 from 0 to 0.014.

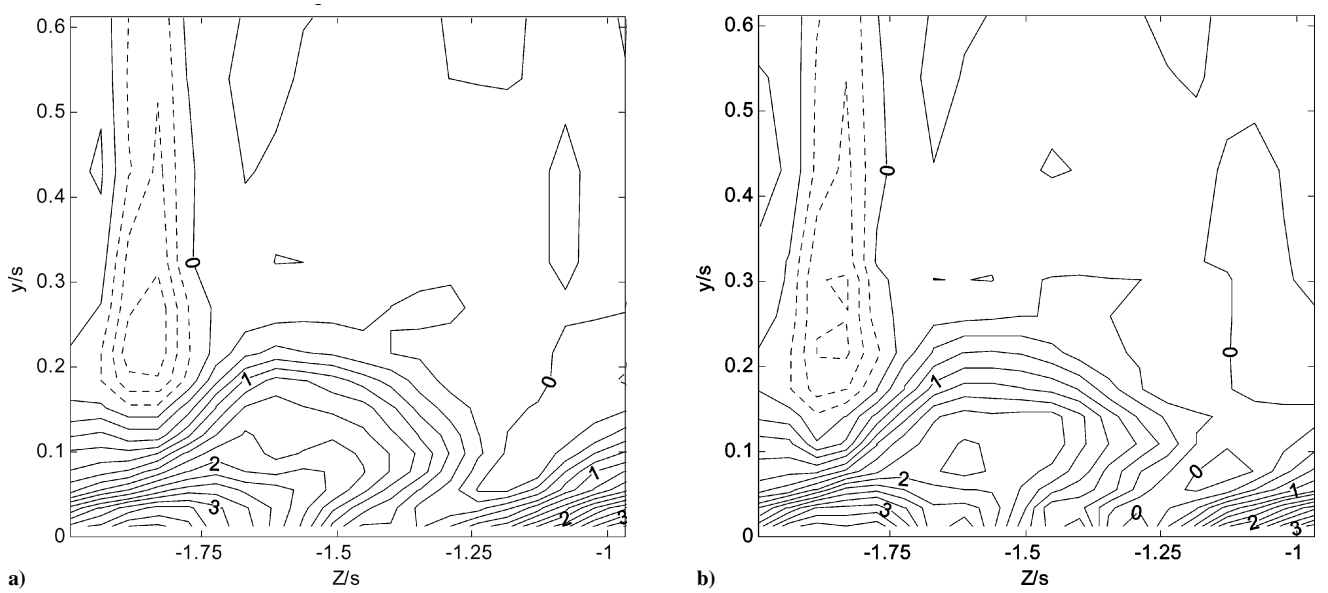

Fig. 10 Contours of streamwise vorticity $\Omega_x s/U_\infty$ at $X/s = 0.944$: a) without vortex generators and b) with vortex generators. Contours are in steps of 0.25 from −5 to 5. Negative levels are shown dashed.

streamwise vorticity. Figures 7a and 7b clearly show the vertical wake of blade 5 on their left-hand edges, centered near $Z/s = -1.85$. Visible at the bottom of these figures is the tip-leakage vortex shed from blade 4 and the associated boundary-layer flow. The tip-leakage vortex is contained within a flattened oval region. Having been convected across the passage, the vortex region intersects with the wake of blade 5. The vortex, $0.25s$ in height, produces a streamwise mean velocity deficit of almost $27\%U_\infty$ at its center for the case without vortex generators and $24\%U_\infty$ for the case with vortex generators. The cross velocity vectors in Fig. 8 reveal a clockwise vortical structure with mean crossflow velocities of about $10\%U_\infty$ associated with its rotation, as well as a strong leakage flow near the wall. The difference between the structures of the vortices is quite small. The fact that the axial-velocity deficit dominates the vortex is probably a characteristic of the light blade loading in this configuration. The vortex is a region of relatively intense turbulent activity. Only small quantitative effects of the vortex generators are visible. The contours of turbulence kinetic energy in Fig. 9 show a slight increase of both level and extent in the vortex core region. The contours of mean streamwise vorticity in Fig. 10 also display a small change in the vortex core with the vortex generators.

Overall the time-averaged TKE production rate[18] has a quite similar distribution both with and without generators. With inflow disturbances, production terms associated with streamwise velocity gradients and those of the rotating secondary flow are a little higher inside the tip-leakage vortex core. Production near the endwall beneath the wake of blade 5 (presumably representing the wake of the leakage jet) is similarly affected. Production terms associated with the secondary flow gradients are enhanced by the disturbances in this region.

The fact that the unsteady vortical inflow produced by the generators does not greatly alter the mean-flow structure is not surprising. Based on inflow measurements we would expect the inflow vortices to be of circulation $0.003U_\infty s$. By comparison, the overall mean circulation in the tip-leakage vortex, computed on a rectangular path extending from $(y/s, Z/s) = (0, -1.884)$ to $(0.323, -1.130)$, is $0.227U_\infty s$, which is about 80 times larger. The important issue here, however, is whether these weak disturbances stimulate coherent unsteadiness in the tip-leakage vortex, and this can only be revealed through phase-averaged measurements.

Cascade Outflow: Phase-Averaged Results

Autospectra were calculated first from the phase-averaged measurement data to examine the nature of the turbulent fluctuations in the tip-leakage vortex. Figure 11 shows the three spectrum components at locations A, B, and C, identified in Fig. 9b. These points are located, respectively, near the moving wall, within the vortex core, and at the top edge of the vortex. Frequency is normalized by the belt speed U_b and blade spacing s. Velocity fluctuations are normalized by nominal inlet freestream velocity U_∞. The spectra clearly show the expected spikes at the generator passing frequency and its first harmonic overlaid on a broadband spectrum. At all three locations this broadband component has a fairly typical turbulent wake form, with signs of an inertial subrange and a diffuse peak at a normalized frequency of between 1 and 2. Very similar peaks at the same frequencies were observed by Wang[33] in his study of the flow downstream of this cascade, but without inflow unsteadiness. He attributed them to organized structures in the leakage vortex. Even though the present spectra show no clear sign of interaction, the frequencies associated with the natural turbulence structure of the vortex are quite close to those associated with the inflow unsteadiness.

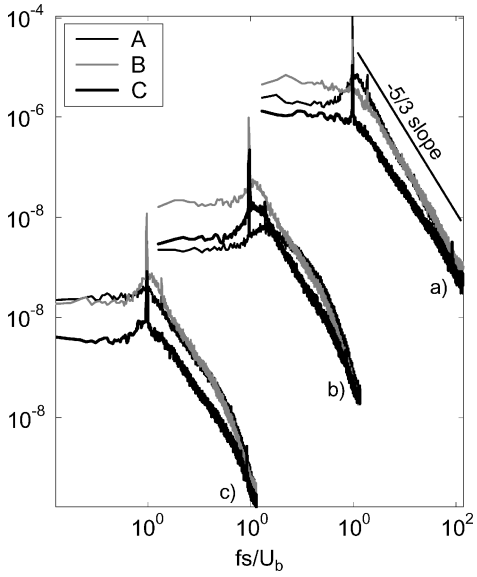

Fig. 11 Autospectra of velocity fluctuations at locations identified in Fig. 9b: a, $G_{uu}U_b/U_\infty^2 s$; b, $G_{vv}U_b/U_\infty^2 s$; and c, $G_{ww}U_b/U_\infty^2 s$.

Phase-averaged results are presented in Figs. 12–14 and Table 2. These show the cross-sectional structure of the flow at eight phases of equal interval corresponding to eight positions of the vortex-generator row. Phase-averaged results of complete 256 phases were

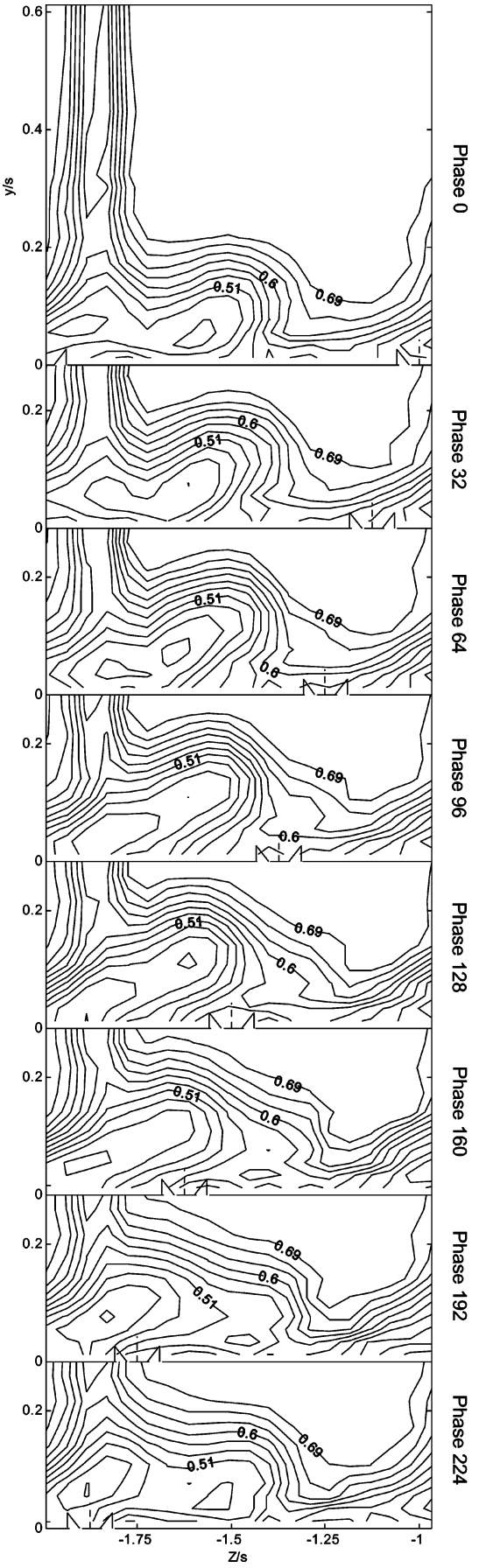

Fig. 12 Contours of phase-averaged streamwise velocity $\langle u \rangle / U_\infty$ at $X/s = 0.944$. Contours are in steps of 0.03 from 0.3 to 0.7. The triangle pairs indicate the picthwise location of vortex generators, which is given in Table 2.

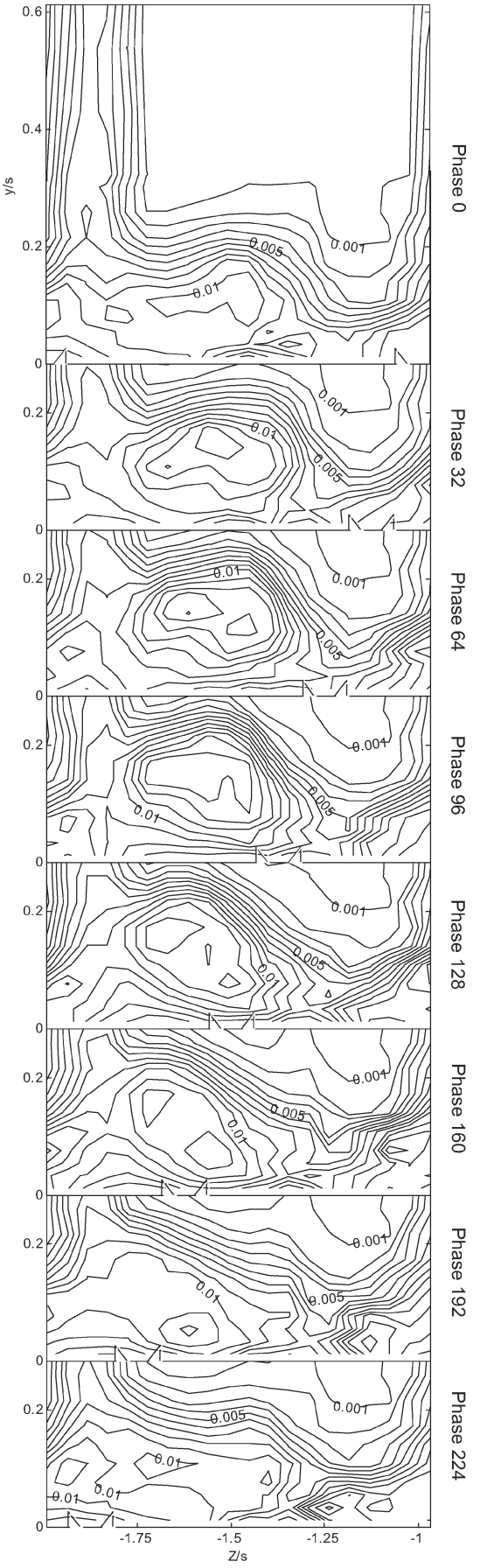

Fig. 13 Contours of phase-averaged turbulence kinetic energy $\langle k \rangle / U_\infty^2$ at $X/s = 0.944$. Contours are in steps of 0.001 from 0 to 0.014. The triangle pairs indicate the picthwise location of vortex generators, which is given in Table 2.

Table 2 Pitchwise location of vortex generators

Phase	Z/s generator	
0	0.000	−1.000
32	−0.125	−1.125
64	−0.250	−1.250
96	−0.375	−1.375
128	−0.500	−1.500
160	−0.625	−1.625
192	−0.750	−1.750
224	−0.875	−1.875

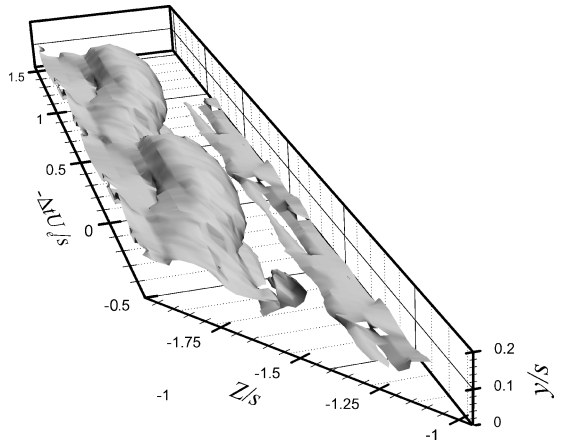

Fig. 14 Contour surface of phase-averaged vortex aligned streamwise vorticity of $1.5U_\infty/s$.

plotted as movies by Ma[18] and can be downloaded from the dissertation website. In our preconceived view of this flow, we expected these cross sections to reveal the counter-rotating inflow vortex pair produced by the generators superimposed upon the tip-leakage vortex, the former traveling in the negative z direction across the endwall with the generators. However, no obvious impression of the counter-rotating vortices appears at any of the phases. Instead, what we observe are phase-locked variations in the position and structure of the tip-leakage vortex. The shape of the tip-leakage vortex, the structure of the vortex core, and the center position all vary with the moving of the vortex generators.

At phase 0 the normalized streamwise velocity component contours shown in Fig. 12 reveal two minima within the tip-leakage vortex both with a deficit of $0.24U_\infty$ relative to the local freestream. The left-hand minimum is located under the wake, and the right-hand minimum is located at $Z/s = -1.6$, $y/s = 0.05$. The contours of normalized turbulence kinetic energy (in Fig. 13) show a peak of 0.01, located a little above the right-hand minimum. As the vortex generators move across the endwall, the left-hand minimum shrinks, and the right-hand minimum extends to the left-hand side. Finally it reaches the left-hand one, and they merge around phase 32. At the same time, the peak normalized turbulence kinetic energy intensifies to 0.012. From phase 32 to 160, the right-hand minimum follows a circuitous process to move to the left-hand side. The deficit first increases to 0.27 as it starts to move to the left. At phase 64, another left-hand minimum is formed. These two minima merge together at phase 96 and finally move to the left-hand side at phase 160. Meanwhile the peak turbulence kinetic energy in this region increases to 0.013, and the turbulence field undergoes a number of changes in its structure, particularly in the core region between $Z/s = -1.7$ and -1.4. From phase 160 to 224, a new minimum is formed at $Z/s = -1.4$ and gradually grows while the minimum at the left-hand side starts to wither. In the meantime, the turbulence kinetic energy inside the vortex core region starts to decay significantly to 0.01, but a peak, formed at the right-hand side, is moving toward the tip-leakage vortex core.

The most obvious explanation of the behavior of the tip-leakage vortex is that it is produced by the direct interaction with the inflow vortices in the blade passage. This ignores the disparity in vortex strength, however, and the fact that the axially aligned inflow vortices must pass through the blade tip gap to reach large parts of the blade passage occupied by the tip-leakage vortex (see Fig. 2). An alternative hypothesis is that the inflow vortices influence the tip-leakage vortex at its formation, by periodically disturbing the shedding of vorticity from the blade tip.

A three-dimensional contour surface of the vortex aligned streamwise vorticity at level of $1.5U_\infty/s$ is plotted in Fig. 14. The Δt axis represents the streamwise coordinate inferred from phase bin number and Taylor's hypothesis based on the potential core velocity downstream of the cascade. The flow of two successive periods was plotted. The contour surface follows a sinuous path with distance downstream and shows no structure that is parallel to the expected axial trajectory of the inflow vortices. This also suggests that there is no direct interaction between the tip-leakage vortex and the inflow vortices.

Tip-Leakage Vortex Center Path

Several methods were attempted to track the tip-leakage vortex center. The first was to calculate the normalized mean helicity density $H = (\boldsymbol{\Omega} \cdot \boldsymbol{V})/(|\boldsymbol{\Omega}||\boldsymbol{V}|)$. The vortex center should lie close to the point where H has a value of 1 or -1, depending on the direction of the vortex. However, it was found the helicity contours did not provide a very clear vortex center location at many phases, but instead showed multiple centers or a center distributed over a range of positions. The streamwise vorticity and the streamwise mean velocity deficit were thus used to track the vortex center. For the former, the maximum streamwise vorticity location inside the tip-leakage vortex region was determined for each phase to reveal the vortex center path. For the latter, the maximum streamwise mean velocity deficit location was used as an indicator of the vortex center position after subtracting the pitchwise-averaged streamwise velocity from the data to minimize the effects of the endwall boundary layer and the leakage flow on the distribution. With either velocity deficit or vorticity as the indicator, there were still phase times when there was more than one vortex center in the tip-leakage region. However, a primary center could still be identified, and it was this that was tracked.

Figure 15 shows the primary tip-leakage vortex center paths indicated by the maximum streamwise vorticity and maximum streamwise velocity deficit. The two methods output similar primary vortex center paths. Starting at phase 213, and continuing through phase 0, the vortex center drifts almost continuously in the negative Z direction, covering a total distance of some $0.3s$. The sudden jump back, at phase 212, simply denotes the formation of a new primary vortex center. The old center rapidly dissipates after this time. The net effect is that the leakage vortex follows a zigzag path, made from a series of component vortices that make an angle with the path of the time-average-vortex center.

This can be seen more clearly in Fig. 16. Here the vortex center location, inferred from the maximum streamwise vorticity, has been plotted in plan view by using the phase time τ_p to estimate relative streamwise position Δx using Taylor's hypothesis, that is, $\Delta x = -\Delta\tau_p U_e$, where U_e was assumed to be the local mainstream velocity. Because the local mainstream velocity is a little higher than the mean velocity averaged over the tip-leakage vortex, the angle of the tip-leakage vortex path to the X axis is probably slightly underestimated. Some additional inaccuracy can be introduced because Taylor's hypothesis is a good approximation only if $u'/U_e \ll 1$, and the streamwise velocity fluctuation is likely quite large in this flow. The figure shows the three-dimensional spatial location of the tip-leakage vortex center path for two successive periods. Both primary vortex center (black line) and nascent vortex center (gray line) are shown in the plot. The photo of the flow visualization of Zierke et al.[12,13] showing the cavitating path of the tip-leakage vortex formed in a propulsion pump rotor with inlet guide vanes is also presented. It can be seen that the zigzag path of the tip-leakage vortex center is consistent with the flow visualization, which shows dramatic wandering and kinking of the cavitating tip-leakage vortex as it passes downstream of the rotor-blade trailing edge. Note that in the present measurements the vortex appears to pass quite close to

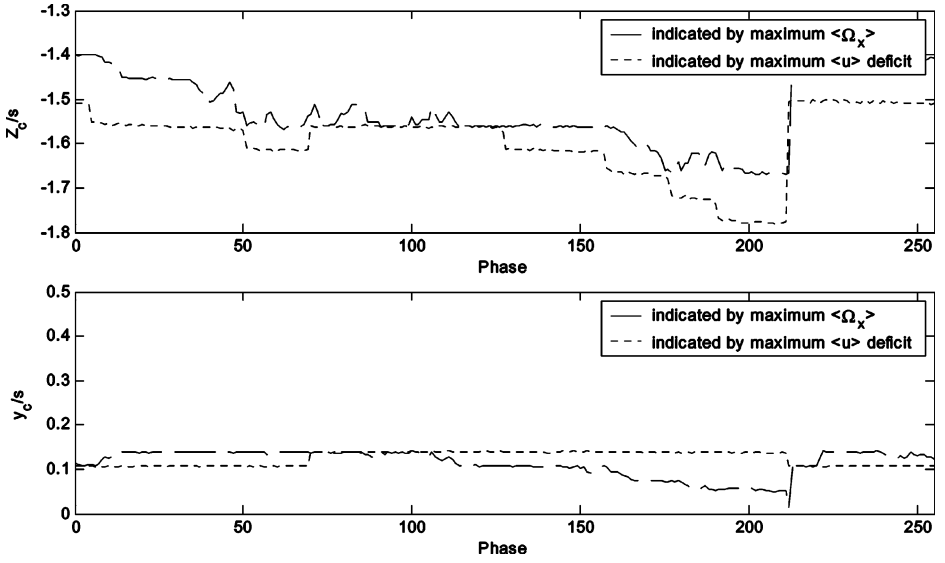

Fig. 15 Primary tip-leakage vortex center locations vs phase for 3.3% chord tip gap.

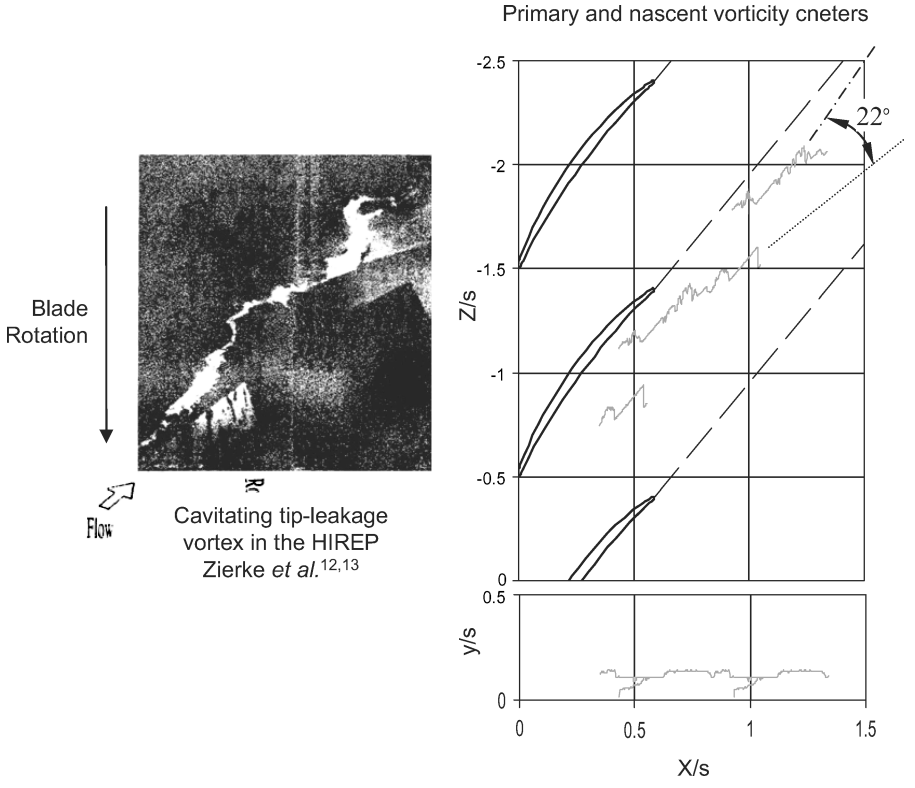

Fig. 16 Three-dimensional spatial location of the tip-leakage vortex center path for 3.3% chord tip gap defined using the peak phase-averaged streamwise vorticity: black line, primary vortex center; gray line, nascent vortex center; –·–·, axis of the tip-leakage vortex; and · · · ·, primary vortex center direction. (The photo on the left is the flow visualization of Zierke et al.[12,13])

the pressure side of the blade following that from which it was shed. The fact that the vortex rapidly crosses the passage is consistent with the measurements of Wang and Devenport[24] made without inflow disturbances.

Wenger et al.[31] also found, through measured three-dimensional space-time correlations, that in the tip-leakage vortex the eddies are skewed at about 30 deg from the axis of the tip-leakage vortex, which is fairly consistent with the angle of 22 deg of current study. Wenger et al.[31] took time-averaged two-point correlation measurements downstream of the same linear compressor cascade at 1.65% chord tip gap but without moving wall and vortex generators. This suggests that the zigzag path of the tip-leakage vortex center is organized not only just by the periodic vortical inflow but also by some mechanism inside the tip-leakage flow turbulence structure itself.

The vortex streamwise stretching $\boldsymbol{\Omega}_i(\partial\langle u\rangle/\partial x_i)$, streamwise vorticity $\boldsymbol{\Omega}_x$, and turbulence kinetic energy k were computed along the vortex center path defined by the maximum streamwise vorticity. Figure 17 presents these properties of the vortex center for the 3.3% chord tip gap case. It can be seen that vortex stretching, streamwise vorticity, and TKE all reach maxima between phases 50 and 150 at which time the vortex center is near the center of its pitchwise excursion.

Two factors are worth considering while examining these results. First, the complete phase cycle represents a time period of $0.236/22.7 = 10$ msc, during which the flow downstream of the cascade convects only about 17 cm ($0.72s$). In other words, the structural changes in the vortex seen here occur over a streamwise length comparable to the vortex width. Second, because this is a strongly turbulent flow (even phase-averaged turbulence intensities

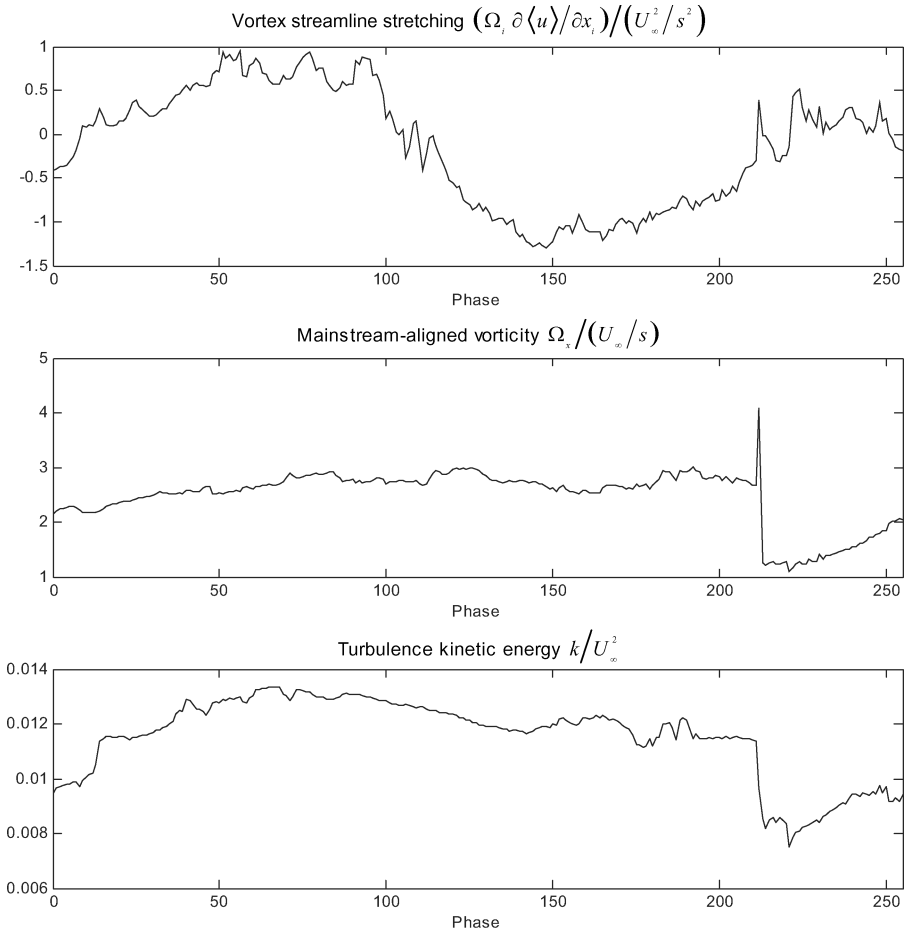

Fig. 17 Phase-averaged tip-leakage vortex center properties for 3.3% chord tip gap, with center based on maximum streamwise velocity deficit.

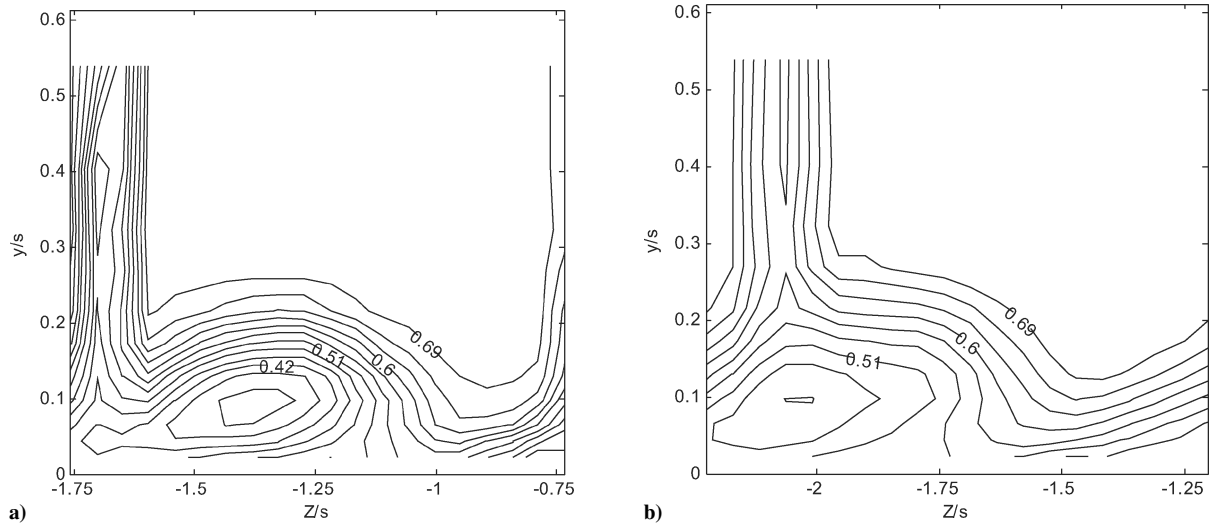

Fig. 18 Contours of time-averaged streamwise velocity U/U_∞: a) at $X/s = 0.772$, and b) at $X/s = 1.117$. Contours are in steps of 0.03 from 0.3 to 0.7.

at the vortex center exceed 25%), it is likely that the instantaneous influence of the inflow vortices upon the tip-leakage vortex is significantly modulated by random turbulent motions. In this way the magnitude of the phase-averaged effects we observe probably substantially underrepresents the magnitude of the instantaneous effects. However, the fact that we see any phase-averaged effect at all is significant. It implies that in true turbomachinery applications rotor tip-leakage flows do undergo coherent unsteady motions produced by the unsteady vortical inflow, even when the unsteadiness is comparatively weak compared to the strength of the tip-leakage flow.

Tip-Leakage Vortex Streamwise Development

The streamwise development of the tip-leakage vortex was studied by conducting phase-averaged hot-wire measurements at two additional locations $X/s = 0.772$ and 1.117 for 3.3%c tip gap. These two locations are in equal distance from the original measurement $X/s = 0.944$, one upstream and other downstream. The data can present the tip-leakage flow in space-time form to reveal the flow structure.

Only the time-averaged contours of streamwise velocity, TKE, and streamwise vorticity are presented here in Figs. 18–20; the phase-averaged data are presented by Ma.[18] The phase-averaged

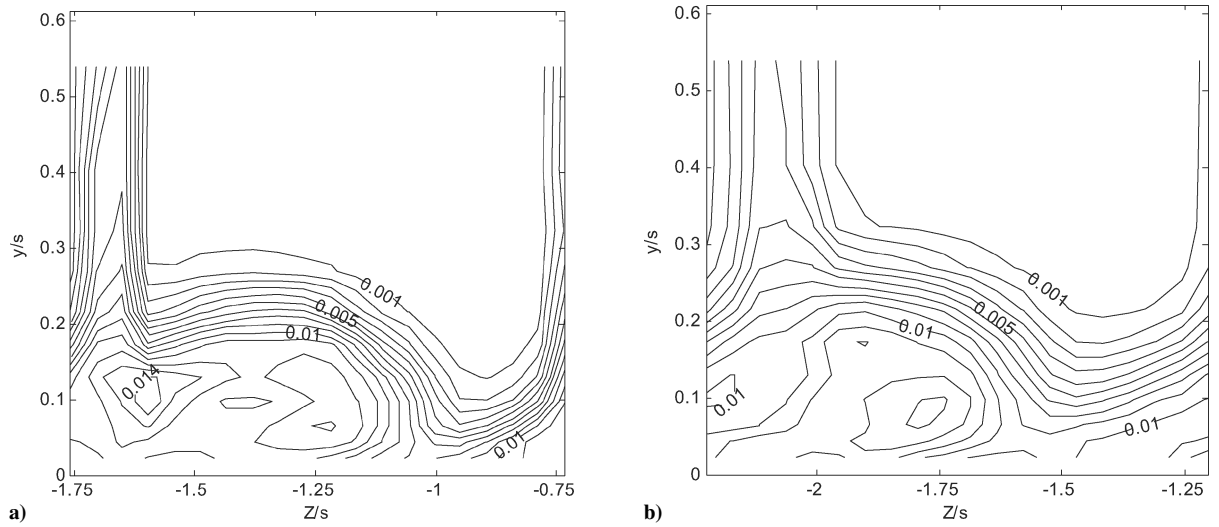

Fig. 19 Contours of time-averaged TKE k/U_∞^2: a) at $X/s = 0.772$ and b) at $X/s = 1.117$. Contours are in steps of 0.001 from 0 to 0.014.

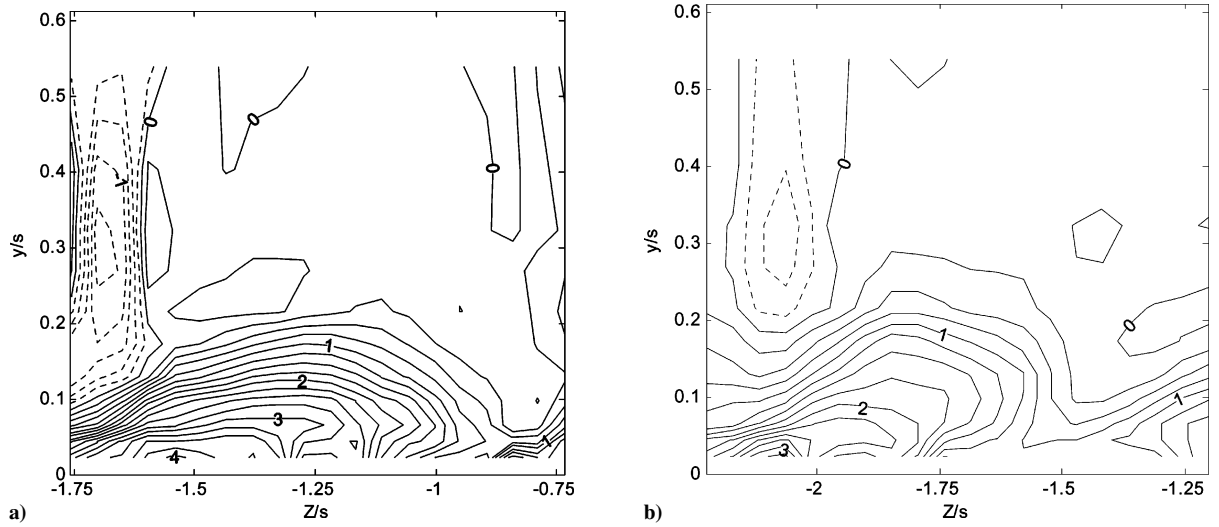

Fig. 20 Contours of time-averaged streamwise vorticity $\Omega_x s/U_\infty$: a) at $X/s = 0.772$ and b) at $X/s = 1.117$. Contours are in steps of 0.25 from −5 to 5. Negative levels are shown dashed.

data at three locations give a full view of the three-dimensional flow structure and how it changes with phase time. It can be seen that streamwise velocity deficit is largest at the upstream section and reduces as flow goes downstream. The contour shapes of the tip-leakage vortex core are also different at three locations even at same phase time. Especially at the two downstream sections the primary vortex center changes significantly with the phase. The real tip-leakage vortex center path also looks perhaps more complicated than that obtained by using Taylor's hypothesis in the last section. TKE is largest in an arc structure that surrounds the top of the vortex core at the upstream station but is largest in the core at the downstream station. This implies that turbulence decays and changes with distance. Similar behavior can be seen in the streamwise vorticity, whose level reduces because of the turbulence decays as the flow goes to the downstream. However, the phase-averaged data show that there is still a very large fluctuation in the vortex shape, structure, and center position at the downstream section.

Conclusions

A linear cascade wind tunnel has been adapted to model the unsteady tip-leakage flow produced by a rotor operating in the vortical wakes of a set of stator vanes. A moving endwall was used to simulate the relative motion between rotor and casing, and vortex generators attached to the moving endwall were used to produce an idealized unsteady inflow. The unsteady periodic behavior of the disturbed tip-leakage vortex was investigated through detailed three-component hot-wire measurements made just downstream of the blade trailing edges and phase averaged with respect to the relative position of the blades and vortex generator wakes.

The unsteady inflow vortices produced by the generators were found to be weak, having a circulation about two orders smaller than that of the tip-leakage vortex and producing an axial-velocity deficit (experienced as an upwash by the cascade blades) over a region only about two tip gaps in height from the endwall. Nevertheless, this inflow was found to have a dramatic influence on the phase-averaged structure of the tip-leakage vortex. Specifically, the vortex was found to undergo large pitchwise excursions in its position, its center following a zigzag path downstream of the rotor-blade trailing-edge plane.

The zigzag motion is accompanied by substantial fluctuations in the structure of the mean flow and turbulence fields generated by the vortex. Vortex stretching, streamwise vorticity, and turbulence kinetic energy at the vortex center all reach maxima when the vortex is near the middle of its pitchwise excursions. Parts of the vortex are seen to divide and recombine during the motion. Because the vortex is a strongly turbulent flow (even phase-averaged turbulence intensities at the vortex center exceed 25%), it is argued the phase-averaged

effects reported on here probably substantially underrepresent the instantaneous effects of the unsteady inflow.

The behavior of the tip vortex suggests there is indirect interaction between the tip-leakage vortex and the inflow vortices. It is hypothesized that the unsteady vortical inflow influences the tip-leakage vortex at its formation, by periodically disturbing the shedding of vorticity from the blade tip.

This paper presents only the first part of data of our investigation. The influence of tip gap, the unsteady aperiodic behavior, and the pressure fluctuations of the tip-leakage vortex will be presented in following papers.

Acknowledgments

The authors thank the Office of Naval Research, in particular Ki-Han Kim, for their support of this work through Grant N00014-99-1-0294. The assistance of Nilanjan Saha and Bancroft Henderson in setting up the wind tunnel and performing measurements is gratefully acknowledged. Numerical results from the experiments described here are available from the authors' website.‡

References

[1]Addison, J. S., and Hodson, H. P., "Unsteady Transition in an Axial-Flow Turbine: Parts 1 and 2," *Journal of Turbomachinery*, Vol. 112, No. 2, 1990, pp. 206–221.

[2]Dong, Y., and Cumpsty, N. A., "Compressor Blade Boundary Layers: Part 2—Measurements with Incident Wakes," *Journal of Turbomachinery*, Vol. 112, No. 2, 1990, pp. 231–241.

[3]Stauter, R. C., Dring, R. P., and Carta, F. O., "Temporally and Spatially Resolved Flow in a Two-Stage Axial Compressor: Part 1—Experiment," *Journal of Turbomachinery*, Vol. 113, No. 2, 1991, pp. 219–226.

[4]Uzol, O., Chow, Y.-C., Katz, J., and Meneveau, C., "Experimental Investigation of Unsteady Flow Field Within a Two Stage Axial Turbomachine Using Particle Image Velocimetry," *Proceedings of ASME TURBO EXPO 2002* [CD-ROM], American Society of Mechanical Engineers, New York, 2002, GT-2002-30664.

[5]Chow, Y.-C., Uzol, O., and Katz, J., "Flow Non-Uniformities and Turbulent 'Hot Spots' due to Wake-Blade and Wake-Wake Interaction in a Multistage Turbomachine," *Proceedings of ASME TURBO EXPO 2002* [CD-ROM], American Society of Mechanical Engineers, New York, 2002, GT-2002-30667.

[6]Poensgen, C., and Gallus, H. E., "Three-Dimensional Wake Decay Inside of a Compressor Cascade and Its Influence on the Downstream Unsteady Flow Field, Part 2 Unsteady Flow-Field Downstream of the Stator," *Journal of Turbomachinery*, Vol. 113, No. 2, 1991, pp. 190–197.

[7]Yamamoto, A., Mimura, F., Tominaga, J., Tomihisa, S., Outa, E., and Matsuki, M., "Unsteady Three-Dimensional Flow Behavior Due to Rotor-Stator Interaction in an Axial Flow Turbine," American Society of Mechanical Engineers, Paper 93-GT-404, May 1993.

[8]Zeschky, J., and Gallus, H. E., "Effects of Stator Wakes and Spanwise Nonuniform Inlet Conditions on the Rotor-Flow," *Journal of Turbomachinery*, Vol. 115, No. 1, 1993, pp. 128–136.

[9]Gallus, H. E., Zeschky, J., and Hah, C., "Endwall and Unsteady Flow Phenomena in an Axial Turbine Stage," American Society of Mechanical Engineers, Paper 94-GT-143, 1994; also *Journal of Turbomachinery*, Vol. 117, No. 4, 1995, pp. 562–570.

[10]Wernet, M. P., John, W. T., Prahst, P. S., and Strazisar, A. J., "Characterization of the Tip Clearance Flow in an Axial Compressor Using Digital PIV," AIAA Paper 2001-0697, Jan. 2001.

[11]Wernet, M. P., Zante, D. V., Strazisar, T. J., John, W. T., and Prahst, P. S., "3-D Digital PIV Measurements of the Tip Clearance Flow in an Axial Compressor," *Proceedings of ASME TURBO EXPO 2002* [CD-ROM], American Society of Mechanical Engineers, New York, 2002, GT-2002-30643.

[12]Zierke, W. C., Farrell, K. J., and Straka, W. A., "Measurements of the Tip Clearance Flow for a High-Reynolds-Number Axial-Flow Rotor," *Journal of Turbomachinery*, Vol. 117, No. 4, 1995, pp. 522–532.

[13]Zierke, W. C., Straka, W. A., and Taylor, P. D., "An Experimental Investigation of the Flow Through an Axial-Flow Pump," *Journal of Fluids Engineering*, Vol. 117, No. 3, 1995, pp. 485–490.

[14]Zierke, W. C., and Straka, W. A., "Flow Visualization and Three-Dimensional Flow in an Axial Pump," *Journal of Propulsion and Power*, Vol. 12, No. 2, 1996, pp. 250–259.

[15]Lee, Y. T., Hah, C., and Loellbach, J., "Three-Dimensional Navier–Stokes Solutions for a One-Stage Axial-Flow Pump," *Proceedings of the 20th Symposium on Naval Hydrodynamics*, National Academy Press, Washington, DC, 1996, p. 1001.

[16]Lee, Y. T., Hah, C., and Loellbach, J., "Flow Analyses in a Single-Stage Propulsion Pump," *Journal of Turbomachinery*, Vol. 118, No. 2, 1996, pp. 240–249.

[17]Hah, C., Loellbach, J. M., and Lee, Y.-T., "Generation and Transport of Tip-Clearance Vortices in a High-Reynolds-Number Axial Flow Rotor," *Computational Fluid Dynamics in Aeropropulsion*, edited by W. Ng, AD-Vol. 49, American Society of Mechanical Engineers, New York, 1995.

[18]Ma, R., "Unsteady Turbulence Interaction in a Tip Leakage Flow Downstream of a Simulated Axial Compressor Rotor," Ph.D. Dissertation, Aerospace and Ocean Engineering Dept., Virginia Polytechnic Inst. and State Univ., Blacksburg, VA, 2003, URL: http://scholar.lib.vt.edu/theses/available/etd-06172003-122153/ [cited 17 June 2003].

[19]Kuhl, D. D., "Near Wall Investigation of Three Dimensional Turbulence Boundary Layer," M.S. Thesis, Aerospace and Ocean Engineering Dept., Virginia Polytechnic Inst. and State Univ., Blacksburg, VA, 2001, URL: http://scholar.lib.vt.edu/theses/available/etd-08212001-222514/ [cited 21 Aug. 2001].

[20]Tain, Q., "Some Features of Tip Gap Flow Fields of a Linear Compressor Cascade," M.S. Thesis, Aerospace and Ocean Engineering Dept., Virginia Polytechnic Inst. and State Univ., Blacksburg, VA, 2001, URL: http://scholar.lib.vt.edu/theses/available/etd-01062004-160730/ [cited 6 Jan. 2004].

[21]Tang, G., "Measurements of the Tip-Gap Turbulent Flow Structure in a Low-Speed Compressor Cascade," Ph.D. Dissertation, Aerospace and Ocean Engineering Dept., Virginia Polytechnic Inst. and State Univ., Blacksburg, VA, 2004, URL: http://scholar.lib.vt.edu/theses/available/etd-05122004-161722/ [cited 12 May 2004].

[22]Mish, P. F., "An Experimental Investigation of Unsteady Surface Pressure on Single and Multiple Airfoils in Turbulence," Ph.D. Dissertation, Aerospace and Ocean Engineering Dept., Virginia Polytechnic Inst. and State Univ., Blacksburg, VA, 2003, URL: http://scholar.lib.vt.edu/theses/available/etd-03312003-173021/ [cited 31 March 2003].

[23]Muthanna, C., and Devenport, W. J., "The Wake of a Compressor Cascade with Tip Gap, Part 1: Mean Flow and Turbulence Structure," *AIAA Journal*, Vol. 42, No. 11, 2004, pp. 2320–2331.

[24]Wang, Y., and Devenport, W. J., "The Wake of a Compressor Cascade with Tip Gap, Part 2: Effects of Endwall Motion," *AIAA Journal*, Vol. 42, No. 11, 2004, pp. 2332–2340.

[25]Pauley, W. R., and Eaton, J. K., "Boundary Layer Turbulence Structure in the Presence of Embedded Streamwise Vortex Pairs," 7th Symposium on Turbulent Shear Flows, Stanford Univ., Paper 5-2, Aug. 1989.

[26]Wittmer, K. S., Devenport, W. J., and Zsoldos, J. S., "A Four-Sensor Hot-Wire Probe System for Three-Component Velocity Measurement," *Experiments in Fluids*, Vol. 24, No. 5–6, 1998, pp. 416–423.

[27]Devenport, W. J., Rife, M. C., Liapis, S. I., and Follin, G. J., "The Structure and Development of a Wing-Tip Vortex," *Journal of Fluid Mechanics*, Vol. 312, April 1996, pp. 67–106.

[28]Kline, S. J., and McClintock, F. A., "Describing Uncertainties in Single Sample Experiments," *Mechanical Engineering*, Vol. 75, No. 1, 1953, p. 3.

[29]Kuhl, D. D., and Simpson, R. L., "Near-Wall Investigation of Embedded Streamwise Vortex Pairs," 10th International Symposium on Applications of Laser Techniques to Fluid Mechanics [CD-ROM], Paper 27.1, Center for Innovation, Technology and Policy Research, Lisbon, July 2000.

[30]Glegg, S. A. L., "The Response of a Swept Blade Row to a Three-Dimensional Gust," *Journal of Sound and Vibration*, Vol. 227, No. 1, 1999, pp. 29–64.

[31]Wenger, C. W., Devenport, W. J., Wittmer, K. S., and Muthanna, C., "The Wake of a Compressor Cascade with Tip Gap, Part 3: Two-Point Statistics," *AIAA Journal*, Vol. 42, No. 11, 2004, pp. 2341–2346.

[32]Muthanna, C., "The Effects of Free Stream Turbulence on the Flow Field Through a Compressor Cascade," Ph.D. Dissertation, Aerospace and Ocean Engineering Dept., Virginia Polytechnic Inst. and State Univ., Blacksburg, VA, 2003, URL: http://scholar.lib.vt.edu/theses/available/etd-08222002-194441/ [cited 22 Aug. 2002].

[33]Wang, Y., "Tip Leakage Flow Downstream of a Compressor Cascade with Moving End Wall," M.S. Thesis, Aerospace and Ocean Engineering Dept., Virginia Polytechnic Inst. and State Univ., Blacksburg, VA, 2000, URL: http://scholar.lib.vt.edu/theses/available/etd-04052000-14200057/ [cited 5 April 2000].

‡ http://www.aoe.vt.edu/flowdata [cited 18 Feb. 2006].

R. So
Associate Editor